Joint Optimization of Radio and Computational Resource Allocation in Uplink NOMA-based Remote State Estimation

Rongzhen Li and Lei Xu *

Posted Date: 1 July 2025

doi: 10.20944/preprints202506.2543.v1

Keywords: Uplink NOMA; outage risk; remote state estimation; coalitioin game; dinkelbach method; successive convex approximation method; dual decomposition method

Article

Joint Optimization of Radio and Computational Resource Allocation in Uplink NOMA-Based Remote State Estimation

Rongzhen Li [†,‡] **and Lei Xu** [*]

School of Computer Science, Nanjing University of Science and Technology (NJUST); 2716101244@qq.com

* Correspondence: xulei_marcus@126.com

† Current address: School of Computer Science and Technology, Nanjing University of Science and Technology, Nanjing, 210094, China.

‡ These authors contributed equally to this work.

Abstract: In industrial wireless networks beyond 5G and toward 6G, combining uplink non-orthogonal multiple access (NOMA) with the Kalman filter (KF) effectively reduces interruption risks and transmission delays in remote state estimation. However, the complexity of wireless environments and concurrent multi-sensor transmissions introduce significant interference and latency, impairing the KF's ability to continuously obtain reliable observations. Meanwhile, existing remote state estimation systems typically rely on oversimplified wireless communication models, unable to adequately handle the dynamics and interference in realistic network scenarios. To address these limitations, this paper formulates a novel dynamic wireless resource allocation problem as a mixed-integer nonlinear programming (MINLP) model. By jointly optimizing sensor grouping and power allocation—considering sensor available power and outage probability constraints—the proposed scheme minimizes both estimation outage and transmission delay. Simulation results demonstrate that, compared to conventional approaches, our method significantly improves transmission reliability and KF estimation performance, thus providing robust technical support for remote state estimation in next-generation industrial wireless networks.

Keywords: Uplink NOMA, outage risk, remote state estimation, coalitioin game, dinkelbach method, successive convex approximation method, dual decomposition method.

1. Introduction

The rapid advancements in beyond 5G and 6G technologies have dramatically improved key aspects of wireless communication, such as bandwidth, latency, and connection density, thereby creating new opportunities for the development of Wireless Sensor Network (WSN) [1–3]. However, these advancements also introduce new challenges, particularly in the efficient management of resources due to limited power, bandwidth constraints, and the complex interactions between critical system components, such as sensor grouping, power allocation, and state estimation. Non-Orthogonal Multiple Access (NOMA), a promising approach for resource sharing, leverages power-domain differentiation to improve system performance, particularly in the uplink. At the same time, Remote State Estimation, often optimized using Kalman filter (KF), is crucial for accurately estimating the system's state, especially under noisy conditions in wireless networks. Despite the potential of both technologies, integrating NOMA with KF based remote state estimation presents unique challenges, including interference management, power control, transmission delay, and outage risks. This paper proposes a joint optimization framework that combines NOMA's resource allocation capabilities with KF for remote state estimation, addressing these challenges simultaneously. By optimizing sensor grouping, power allocation, and transmission strategies, this approach minimizes outage risks while enhancing both the accuracy of remote state estimation and transmission efficiency, ensuring better system performance and sustainability in beyond 5G and 6G technologies.

 doi:10.20944/preprints202506.2543.v1

During the transmission of sensor local states to the base station, limitations in bandwidth, power, and other resources, as well as factors such as delay, packet loss, and channel interference, make it a critical issue to consider how to assign sensors to channels and set appropriate power levels for each sensor to minimize the total outage risk across all sensors. To address this, we propose combining game theory with sensor grouping and power allocation strategies in NOMA as an effective approach [4–6]. For instance, Liu et al. propose a greedy subchannel matching algorithm based on hypergame theory for sensor and subchannel pairing in downlink NOMA networks, highlighting the importance of sensor grouping in WSN [7]. Additionally, a game-theory-driven data security transmission method is proposed to mitigate potential interference in drone-assisted vehicular networks, with the significant impact of mutual interference on communication quality being demonstrated [8]. Wang et al. explore the application of game theory in cooperative communication scenarios, proposing a two-stage game model based on power and spectrum trading, optimizing transmission rates by solving the game equilibrium, and emphasizing the key role of power in communication processes [9,10].

While some models in sensor wireless transmission are convex functions, many others are non-convex, which makes traditional game-theory methods ineffective in solving such problems. As a result, researchers have proposed solutions to convert non-convex problems into convex optimization problems [11–13]. For example, In reference [14], a joint optimization algorithm that combines the Dinkelbach algorithm with successive convex approximation (SCA) method, successfully converting fractional optimization problems into equivalent linear problems, thus converting non-convex problems into convex ones. This method proves the existence of an optimal solution for the joint optimization of power and subcarrier allocation. The complex constrained optimization problems are simplified using Lagrangian dual decomposition in [15,16], where power allocation in uplink NOMA systems is optimized, leading to a significant reduction in computational complexity. Transmission delay is another critical factor. Transmission delay, energy consumption, and sensor grouping are jointly optimized in [17,18], where their impacts on data transmission are studied, emphasizing the indispensable role of transmission delay in the optimization process.

Although existing research provides valuable insights into addressing some problems in sensor wireless transmission, several challenges remain unsolved. First, effectively integrating transmission delay, energy consumption, channel interference, and outage risk due to remote state estimation in beyond 5G and 6G environments remains a complex problem. Second, while some methods have addressed parts of non-convex optimization problems, further research is needed to reduce system complexity while maintaining computational efficiency. Additionally, current game-theory models primarily focus on single-objective optimization; thus, balancing multiple objectives in a multi-objective optimization framework requires further exploration.

Minimizing outage risks for sensors during transmission is critical for ensuring the stability and reliability of uplink NOMA systems [19–21]. Yadav et al. introduce the optimization of intelligent reflecting surface reflection coefficients, which effectively reduces the impact of channel fading and lowers outage probability [22]. However, it does not fully address the effects of power allocation and non-ideal intelligent reflecting surfaces on the system. Power allocation and sensor grouping are optimized in [23] to reduce outage risks and increase system capacity, though the study lacks a detailed discussion of interference management and dynamic resource scheduling strategies. In [24], outage probability in downlink NOMA systems is minimized through energy harvesting and cooperative communication optimization; however, the paper does not explore how to further improve performance via enhanced CSI estimation and optimized power allocation. The optimization of power allocation is used to enhance system rate and reduce outage probability, though the specifics of sensor grouping and interference management are not delved into in the study [25]. Overall, while these methods effectively reduce outage probability, they do not fully explore refined resource scheduling strategies. Future research could investigate the impact of these factors on system performance.

When addressing the minimization of outage risk during the remote state estimation process for sensors, we must not only consider sensor state estimation issues (e.g., the state estimation error

 doi:10.20944/preprints202506.2543.v1

covariance in [26]), but also focus on the communication challenges in beyond 5G and 6G wireless transmission. Unlike conventional studies that rely purely on quality-of-service (QoS) metrics or signal-to-interference-plus-noise ratio (SINR) for sensor grouping and power allocation, this work focuses explicitly on integrating remote state estimation, network communication processes, and outage probabilities during transmission. Specifically, the complexity arises from the necessity to balance multiple performance criteria—remote state estimation accuracy, transmission latency, and outage probability—in a unified optimization framework, which underscores the importance of jointly utilizing uplink NOMA and KF techniques. The main contributions of this paper are summarized as follows

1. **Problem Modeling:** We propose a novel unified optimization framework, formulating the joint minimization of outage risk in remote state estimation and transmission delay as a mixed-integer nonlinear programming (MINLP) problem. This formulation explicitly incorporates both communication and estimation constraints, providing a theoretical foundation for subsequent algorithm designs..
2. **Coalitional Game-Based Sensor Grouping:** Motivated by the limitations of traditional heuristic approaches, we propose a coalitional game-based sensor grouping algorithm. This algorithm allows sensors to adaptively form cooperative groups, effectively addressing the interference problem in multi-sensor uplink scenarios and significantly improving grouping efficiency and resource utilization.
3. **Power Allocation Optimization:** To handle the nonlinearity and non-convexity inherent in the formulated optimization problem, we apply the Dinkelbach algorithm to convert the original optimization into a parametric form, then solve it via SCA and dual decomposition techniques. This approach achieves an efficient and scalable solution with significantly reduced computational complexity.

By combining these strategies, our framework effectively mitigates outage risks during sensor transmissions and considerably enhances overall system reliability and estimation performance. Additionally, by transforming the original non-convex optimization into convex subproblems, the proposed solution methodology substantially reduces computational complexity. These contributions provide theoretical insights and practical guidelines for optimizing wireless transmission in uplink NOMA systems within future industrial wireless networks beyond 5G and 6G.

The remainder of the paper is organized as follows: Section II presents the mathematical formulation of the problem, Section III investigates the coalition game-based sensor grouping problem and the joint optimization algorithm for solving the optimal power allocation, while numerical examples and conclusions are presented in Sections IV and V, respectively.

Notations: $\mathbb{R}$ denotes the set of real numbers. $\mathbb{C}$ represents the set of complex numbers. The symbol $(\cdot)^T$ denotes the transpose operation. The superscript $(\cdot)^{-1}$ indicates the matrix inverse. The symbol $(\cdot)'$ represents the vector or matrix transpose operator. The notation $\mathbb{P}[\cdot]$ refers to probability. $\mathrm{Tr}(\cdot)$ represents the trace operator of a matrix.

2. System Model

This paper investigates an uplink NOMA transmission model in a wireless sensor network with a single base station. As illustrated in Figure 1, after performing local processing, N sensors transmit their data to the base station, which subsequently conducts remote state estimation. Before transmission, each sensor independently evaluates and selects one of the G channels for sensor grouping based on a comprehensive assessment of factors such as its distance to the base station, channel gain, maximum and minimum power constraints, and noise levels. Additionally, within each group, the decoding order and power allocation strategy are determined to optimize transmission performance and resource utilization efficiency. This process highlights the sensors' adaptive capabilities in channel selection, grouping, and resource scheduling, which are critical components of the system design. The set of cellular sensors is denoted by $\mathcal{N} = \{1, 2, \ldots, N\}$, with each sensor equipped with a single antenna.

 doi:10.20944/preprints202506.2543.v1

In an uplink NOMA system for beyond 5G and 6G networks, the same channel can be assigned to multiple sensors. It is assumed that all sensors in the base station share $\mathcal{G}$ channels, resulting in $\mathcal{G} = \{1, 2, \ldots, G\}$ NOMA clusters within the cell. The set of sensor numbers in each cluster is defined as $\mathcal{I} = \{1, 2, \ldots, I\}$.

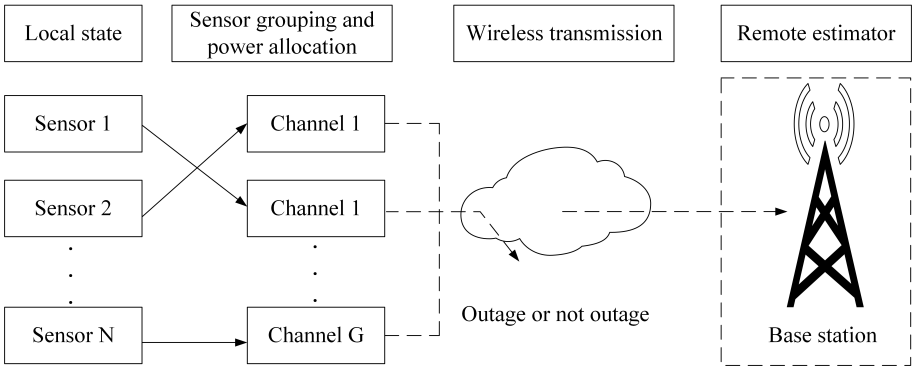

Figure 1. System model of remote state estimation outage risk

2.1. Local State Estimate Model

To introduce the basic framework of the KF method, we describe how the measurement output of sensor i in channel g reflects the underlying process. The system's state at the next time step evolves from the previous state at time t according to the linear transition equation

$$x_{i,g}^{t+1} = A_i^g x_{i,g}^t + w_{i,g}^t, \tag{1}$$

where $x_{i,g}^t \in \mathbb{R}^{l_n}$, $w_{i,g}^t \in \mathbb{R}^{l_n}$, and $A_i^g \in \mathbb{R}^{l_n \times l_n}$ is the state transition matrix. The state variable $x_{i,g}^{t+1}$ and the process noise $w_{i,g}^t$ are independent and follow complex Gaussian distributions. At the next time step, the observation is modeled by the linear measurement equation

$$y_{i,g}^{t+1} = C_i^g x_{i,g}^t + v_{i,g}^t, \tag{2}$$

where $y_{i,g}^{t+1} \in \mathbb{R}^{r_n}$, $C_i^g \in \mathbb{R}^{r_n \times l_n}$ is the measurement matrix, and $v_{i,g}^t \in \mathbb{R}^{r_n}$ is the measurement noise, which also follows a complex Gaussian distribution [27,28]. The KF aims to use a sequence of observations to accurately estimate the state.

The prior and posterior state estimates, $\hat{x}_{i,g}^{t|t-1}$ and $\hat{x}_{i,g}^t$, respectively, are updated using the Kalman gain $K_{i,g}^t$ and the error covariances $P_{i,g}^{t|t-1}$ and $P_{i,g}^t$. The KF equations are as follows [26]

$$\hat{x}_{i,g}^{t|t-1} = A_i^g \hat{x}_{i,g}^{t-1}, \tag{3}$$

$$P_{i,g}^{t|t-1} = A_i^g P_{i,g}^{t-1} (A_i^g)' + Q_i^g, \tag{4}$$

$$K_{i,g}^t = P_{i,g}^{t|t-1} (C_i^g)' \left[C_i^g P_{i,g}^{t|t-1} (C_i^g)' + R_i^g \right]^{-1}, \tag{5}$$

$$\hat{x}_{i,g}^t = \hat{x}_{i,g}^{t|t-1} + K_{i,g}^t \left(y_{i,g}^t - C_i^g \hat{x}_{i,g}^{t|t-1} \right), \tag{6}$$

$$P_{i,g}^t = \left(\nu - K_{i,g}^t C_i^g \right) P_{i,g}^{t|t-1}, \tag{7}$$

where ν is the identity matrix of size $l_n \times l_n$.

The estimation error covariance, denoted $P_{i,g}^t$, quantifies the uncertainty of the state estimate and is defined as

$$P_{i,g}^t \triangleq \mathbb{E}\left[\left(x_{i,g}^t - \hat{x}_{i,g}^t \right) \left(x_{i,g}^t - \hat{x}_{i,g}^t \right)' \right]. \tag{8}$$

 doi:10.20944/preprints202506.2543.v1

As the local estimation error covariance $P_{i,g}^t$ converges exponentially to a steady-state value $\bar{P}_i^g$, the KF's accuracy improves over time.

2.2. Uplink NOMA Communication Model

The impulse response of the channel between sensor i and the base station is represented by $h_{i,g}^k = \frac{e_{i,g}^k}{\sqrt{1+(d_{i,g}^k)^\beta}}$, where $e_{i,g}^k$ denotes the impulse response of the Rayleigh fading channel, with β as the path loss exponent and $d_{i,g}^k$ as the distance between sensor i and the base station. The probability density function of $|e_{i,g}^k|^2$ is given by $f_{|e_{i,g}^k|^2}(x) = \frac{1}{2\mu^2} e^{-\frac{x}{2\mu^2}}$, where μ is the variance of the normal distribution $N(0, \mu)$.

The received signal at the base station is given by

$$y_g^k = \sum_{i=1}^{I} h_{i,g}^k \sqrt{p_{i,g}^k} s_{i,g}^k + n_g, \tag{9}$$

where $p_{i,g}^k$ represents the transmit power allocated to sensor i in channel g, and $s_{i,g}^k$ denotes the transmitted message from sensor i in channel g. Additionally, n_g represents the Gaussian white noise in the process of signal transmission from the base station to sensor i through channel g.

The probability density function (PDF) of $|e_i|^2$ [19] is given by

$$F_{\left|e_{i,g}^k\right|^2}(x) = \int_{-\infty}^{x} f_{\left|e_{i,g}^k\right|^2}(t)dt = 1 - e^{-\frac{x}{2\mu^2}}. \tag{10}$$

At the receiver in a NOMA system, SIC detection is applied to separate the multi-sensor superimposed signals. The optimal decoding order follows an ascending sequence based on sensors' channel gains, allowing for sequential detection and separation of each sensor's signal. Finally, the achievable transmission rate for sensor i in channel g can be expressed according to Shannon's theorem as follows: At the receiver in a NOMA system, SIC detection is applied to separate the multi-sensor superimposed signals. The optimal decoding order is determined by an ascending sequence of sensors' channel gains, thereby facilitating sequential detection and the separation of each sensor's signal. Finally, the achievable transmission rate for sensor i in channel g can be expressed according to Shannon's theorem as follows

$$R_{i,g}^k = B \log_2(1 + \mathrm{SINR}_{i,g}^k), \tag{11}$$

where B represents the bandwidth available to each sensor and $\mathrm{SINR}_{i,g}^k$ is defined as $\frac{p_{i,g}^k |h_{i,g}^k|^2}{\sum_{j=i+1}^{I} p_{j,g}^k |h_{j,g}^k|^2 + \sigma^2}$.

The outage probability, as a critical metric for evaluating wireless system performance, represents the probability that the instantaneous link rate falls below the required sensor rate. We define $E_{i,g}^k$ as the event in which the base station can successfully decode the signals from sensors 1 to $i-1$ in channel g but fails to correctly decode the signal from sensor i in the same channel. When the sensor's rate requirement is $R_{i,g}^k$, the minimum transmission rate is $\hat{R}_{i,g}^k$, and $R_{i,g}^k < \hat{R}_{i,g}^k$, the outage probability of the event $E_{i,g}^k$ can be expressed as follows [21]

$$\mathbb{P}(E_{i,g}^k) = \mathbb{P}\left\{R_{i,g}^k < \hat{R}_{i,g}^k\right\} = 1 - e^{-\frac{\phi_{i,g}^k}{2\mu^2}}, \tag{12}$$

 doi:10.20944/preprints202506.2543.v1

where $\phi_{i,g}^k = \frac{(2^{\frac{\hat{R}_{i,g}^k}{B}}-1)(\sum_{j=i+1}^{I} p_{j,g}^k |h_{j,g}^k|^2+\sigma^2)\left(1+(d_{i,g}^k)^\beta\right)}{p_{i,g}^k}$. Correspondingly, this also represents its non-outage probability, which we define as $\mathbb{P}_c$. Based on the above derivation, the outage probability for sensor i in channel g is formulated as follows

$$\mathbb{P}_{i,g}^{out,k} = 1 - \mathbb{P}_c(E_{1,g}^k \cap \cdots \cap E_{i,g}^k) = 1 - \prod_{z=1}^{i} e^{-\frac{\phi_{z,g}^k}{2\mu^2}}, \tag{13}$$

where

$$\phi_{z,g}^k = \begin{cases} \frac{(2^{\frac{R_{z,g}^k}{B}}-1)(\sum_{j=z+1}^{I} p_{j,g}^k |h_{j,g}^k|^2+\sigma^2)\left(1+(d_{z,g}^k)^\beta\right)}{p_{z,g}^k}, & z \neq I, \\ \frac{(2^{\frac{R_{z,g}^k}{B}}-1)\left(1+(d_{z,g}^k)^\beta\right)\sigma^2}{p_{z,g}^k}, & z = I. \end{cases}$$

2.3. Remote State Estimation Model

At each remote time k, all sensors must send their local estimates to the remote estimator over a shared wireless channel. We denote the transmission of $\hat{x}_{i,g}^k$ by a binary random process $\left\{\gamma_{i,g}^k\right\}$ (see Algorithm 1)

$$\gamma_{i,g}^k = \begin{cases} 1, & \text{if } \hat{x}_{i,g}^k \text{ arrives without errors at time } k, \\ 0, & \text{otherwise (regarded as dropout)}. \end{cases} \tag{14}$$

Let $P_{i,g}^{r,k}$ represent the outage risk covariance for the remote state estimation of sensor i in channel g. When the local estimate is unavailable, the estimator predicts $P_{i,g}^{r,k}$ as follows:

$$P_{i,g}^{r,k} = \begin{cases} \bar{P}_i^g, & \text{if } \gamma_{i,g}^k = 1, \\ A_i^g\left(P_{i,g}^{r,k-1}\right)(A_i^g)' + Q_i^g, & \text{if } \gamma_{i,g}^k = 0. \end{cases} \tag{15}$$

Combining Equation (14) with Equation (13) from the previous section, we can draw the following conclusion

$$\mathbb{P}\left[\gamma_{i,g}^k = 0\right] = 1 - \prod_{z=1}^{i} e^{-\frac{\phi_z^g}{2\mu^2}}. \tag{16}$$

2.4. Transmission Delay Model

2.4.1. Local Transmission Time

When sensor i in channel g performs its task locally, the task execution delay can be described by

$$T_{i,g}^{local} = \frac{I_i^g}{F^s}. \tag{17}$$

where F^s denotes the computational capability of the sensor.

2.4.2. Base Station Offload and Processing Time

If the sensor offloads its task to the base station, the total delay consists of the transmission delay over the wireless link and the execution delay at the base station, expressed as

$$T_{i,g}^{off} = T_{i,g}^{tra} + T_{i,g}^{base}, \tag{18}$$

where $T_{i,g}^{tra}$ and $T_{i,g}^{base}$ denote the transmission delay and the execution delay, respectively. The transmission delay is formulated as

$$T_{i,g}^{tra} = \frac{D_i^g}{R_i^g}. \tag{19}$$

 doi:10.20944/preprints202506.2543.v1

and the execution delay at the base station is

$$T_{i,g}^{base} = \frac{I_i^g}{F^b}, \tag{20}$$

where F_b denotes the computational capability of the base station. The total time expenditure for the sensor is

$$T_{i,g}^{total} = T_{i,g}^{local} + T_{i,g}^{off}. \tag{21}$$

2.5. Problem Formulation

In this section, we formulate an optimization problem to minimize the remote outage risk, which incorporates the total time expenditure and the associated error covariance of remote state estimation in KF. The objective is to jointly optimize sensor grouping and power allocation for the sensors. Specifically, we define the system's objective value using the following equation

$$\begin{aligned} \mathbf{J}_{i,g}^k = \mathrm{Tr}\{&(1-\mathbb{P}_{i,g}^{out,k})[\xi T_{i,g}^{total,k} + (1-\xi)\psi \bar{P}_i^g] \\ &+ \mathbb{P}_{i,g}^{out,k}[\xi T_{i,g}^{local,k} + (1-\xi)\psi H_i^g(P_{i,g}^{r,k-1})]\}, \end{aligned} \tag{22}$$

where $H_i^g(X) \triangleq A_i^g X (A_i^g)' + Q_i^g$ and ξ (with $0 < \xi < 1$) is a weight factor used to combine the objectives into a single function, and ψ is a scaling factor to align the objectives to the same magnitude. The description of Problem 1 is as follows

$$\text{Problem 1:} \min_{p_{i,g}^k} \frac{1}{K} \sum_{k=1}^{K} \sum_{i=1}^{I} \sum_{g=1}^{G} \mathbf{J}_{i,g}^k \tag{23a}$$

$$\text{s.t.} \quad p_{i,g}^k \le p_{\max}, \quad i \in \mathcal{I}, g \in \mathcal{G}, \tag{23b}$$

$$T_{i,g}^{total,k} \le T_{i,g}^{max}, \quad i \in \mathcal{I}, g \in \mathcal{G}, \tag{23c}$$

$$\bigcup_{i \in \mathcal{I}} \bigcup_{g \in \mathcal{G}} \mathcal{U}_i^g = \mathcal{N}, \quad i \in \mathcal{I}, g \in \mathcal{G}, \tag{23d}$$

$$\mathcal{U}^g \cap \mathcal{U}^{g'} = \varnothing, \quad g, g' \in \mathcal{G}, \tag{23e}$$

Constraint (23b) specifies that the transmission power of sensor i in channel g must be lesser than the maximum transmission power limits. Constraint (23c) ensures that the overall transmission time experienced by sensor i over channel g does not exceed the prescribed maximum threshold. Constraints (23d) and (23e) indicate that each sensor can be assigned to only one channel.

3. Solution of the Optimization Probelm

In this chapter, we propose an optimization method based on algorithm decomposition for the MINLP problem in Problem 2. Due to the high computational complexity typically associated with solving MINLP problems, we decompose the original problem into two subproblems to reduce the computational burden during the solution process, aiming to improve both the solving efficiency and practical feasibility of the implementation.

 doi:10.20944/preprints202506.2543.v1

Algorithm 1 Iterative Algorithm Based on KF Method

Input: $A_i^g, C_i^g, Q_i^g, R_i^g, w_{i,g}^t, v_{i,g}^t, \epsilon, t_{\max}$.
Output: $\bar{P}_i^g$, $P_{i,r}^g(k)$.
Initialization: $t = 1, \Delta = 1$.

while $\Delta > \epsilon$ **or** $t \leq t_{\max}$ **do**
  Calculate $P_{i,g}^t$ according to formula (3),(4),(5),(6),(7)
  Update $\Delta = P_{i,g}^t - P_{i,g}^{t-1}$
  Update $t = t + 1$
end while
Obtain $\bar{P}_i^g = P_{i,g}^k$
for $k = 1$ to K **do**
  for $i = 1$ to I **do**
    for $g = 1$ to G **do**
      Set $\gamma_{i,g}^k \in \{0, 1\}$
      if $\gamma_{i,g}^k = 1$ **then**
        $P_{i,g}^{r,k} = \bar{P}_i^g$
      else
        $P_{i,g}^{r,k} = A_i^g \left(P_{i,g}^{r,k-1}\right)(A_i^g)' + Q_i^g$
      end if
    end for
  end for
end for

3.1. Grouping Strategy Based on Coalition Game Theory

To obtain the initial grouping $\mathcal{U}_{ini}$, sensors are uniformly and randomly assigned to each channel, achieving an even distribution of sensors across channels (see Algorithm 2).

In the above system model, the sensors are divided into multiple channels, each forming a coalition of the same size. Within each coalition, sensors collaboratively offload their respective data blocks to the base station, while competition exists between different coalitions. The objective of the optimization problem is to maximize the overall system performance. We define the outage risk under the joint optimization of remote state estimation and transmission delay as the utility function v within the coalition, representing the total outage risks of all sensors within the coalition, as follows

$$v(\mathcal{G}) = (\mathbb{O}_1, \mathbb{O}_2, \cdots, \mathbb{O}_N). \tag{24}$$

Before the matching process, the mutual preference lists are indispensable. Both sensors and base station need to build their preference lists based on their own utilities. We define Γ as the total outage risks of all sensors within a coalition. For any sensors $\mathcal{U}_i^g \in \mathcal{N}, \mathcal{U}_j^{g'} \in \mathcal{N}$, with $\mathcal{U}_i^g \in G_g$ and $\mathcal{U}_j^{g'} \in G_{g'}$, $G_g \succ_{\mathcal{U}_i^g, \mathcal{U}_j^{g'}} G_{g'}$ indicates that sensor $\mathcal{U}_i^g$ prefers joining coalition G_g over $G_{g'}$. In this case, the sensor will exchange positions with those in $G_{g'}$. The final result is that, after exchanging positions, the total outage risks of sensors in different coalitions is higher than before the exchange. The new partition can be denoted as $\Gamma\{\mathcal{G}'\} = \Gamma(G_g \setminus \{\mathcal{U}_i^g\} \cup \{\mathcal{U}_j^{g'}\}) + \Gamma(G_{g'} \setminus \{\mathcal{U}_j^{g'}\} \cup \{\mathcal{U}_i^g\})$.

 doi:10.20944/preprints202506.2543.v1

Algorithm 2 Intelligent Sensor Grouping Algorithm Based on Coalition Game Theory under Fixed Power Constraints

Input: $\mathcal{N}, \mathcal{G}^0, \mathcal{I}, h_i^g, p_i^g, n \in \mathcal{N}, i \in \mathcal{I}, g \in \mathcal{G}^0$.
Output: Optimal grouping $\mathcal{G}_{fin}$.
Initialization: $t = 1$, $p_i^g = p_{\max}$, $\mathcal{U}_{ini} = \mathcal{U}_i^g$, $\mathcal{G}^0 = \mathcal{G}_{ini}$, $\forall i \in \mathcal{I}$, $g \in \mathcal{G}^0$.

while $\mathcal{G}^t$ does not converge to Nash-stable partition G_{fin} **do**
  Select $\mathcal{U}_i^g \in G_g$ and $\mathcal{U}_j^{g'} \in G_{g'}$, where $g \neq g', i \in \mathcal{I}, j \in \mathcal{I}$
  Define $\mathcal{G}' = \left(\mathcal{G}^t \setminus \{G_{g'}, G_g\}\right) \cup \{G_{g'} \setminus \{\mathcal{U}_i^g\} \cup \{\mathcal{U}_j^{g'}\}, G_g \setminus \{\mathcal{U}_j^{g'}\} \cup \{\mathcal{U}_i^{g'}\}\}$
  Calculate $\mathbb{E}(G_m), \mathbb{E}(G_{m'})$ by Problem 4
  if $\Gamma\{\mathcal{G}'\} > \Gamma\{\mathcal{G}^t\}$ **then**
    Update $\mathcal{G}^{t+1} = \mathcal{G}'$
    Update $t = t + 1$
  end if
end while

3.2. Power Allocation Based on Dinkelbach, SCA, and Dual Decomposition Methods

This section addresses the power allocation problem for a fixed sensor grouping by applying the Dinkelbach algorithm, along with the SCA and dual decomposition methods discussed below. To address the issue of offloading time consumption in the expectation, we use the Dinkelbach algorithm to handle the fractional programming. The transformed problem is described as follows (see Algorithm 3)

$$\mathbf{J}_{i,g}^k = \mathrm{Tr}\left\{ Z_{i,g}^k - \prod_{z=1}^{i} e^{-\frac{\phi_{z,g}^k}{2\mu^2}} \left(\lambda_{i,g}^k \frac{R_{i,g}^k}{\xi} + L_{i,g}^k \right) \right\}. \tag{25}$$

where $Z_{i,g}^k$ and $L_{i,g}^k$ represent $\xi T_{i,g}^{local,k} + (1-\xi)\psi \bar{P}_i^g$ and $(1-\xi)\psi Z_{i,g}^k - D_i^g - \xi T_{i,g}^{base,k}$, respectively, and $\lambda_{i,g}^k$ is a non-negative parameter. We define $F(\lambda_{i,g}^k) = -\min\limits_{p_{i,g}^k} \left\{ \lambda_{i,g}^k \frac{R_{i,g}^k}{\xi} - D_i^g \right\}$.

Algorithm 3 Iterative Algorithm Based on Dinkelbach

Input: $\xi, D_i^g, R_{i,g}^k$, iter_max, $\epsilon, i \in \mathcal{I}, g \in \mathcal{G}$.
Initialization: $\lambda_{i,g}^{\mathrm{iter},k} = 0$, iter $= 1$.

while $F(\lambda_{i,g}^{\mathrm{iter},k}) > \epsilon$ **or** iter $\leq$ iter_max **do**
  $F(\lambda_{i,g}^{\mathrm{iter},k}) = D_i^g - \lambda_{i,g}^{\mathrm{iter},k} \frac{R_{i,g}^k}{\xi}$
  iter $=$ iter $+ 1$
  $\lambda_{i,g}^{\mathrm{iter},k} = \xi \frac{D_i^g}{R_{i,g}^k}$
end while

Output: Obtain $\lambda_{i,g}^k = \lambda_{i,g}^{\mathrm{iter},k}$.

To facilitate subsequent analysis, we can derive from Equation (25) that the minimization problem above can be transformed into a maximization problem. Additionally, since $Z_i^g(k)$ is a constant, it has no impact on sensor grouping or power allocation. we redefine an objective function $\mathbf{O}_{i,g}^k$, which is derived from the original objective function $\mathbf{J}_{i,g}^k$ by excluding the $Z_{i,g}^k$ component and can be considered an approximation of $\mathbf{J}_{i,g}^k$.

$$\mathbf{O}_{i,g}^k \approx -\mathbf{J}_{i,g}^k = \mathrm{Tr}\left\{ \prod_{z=1}^{i} e^{-\frac{\phi_{z,g}^k}{2\mu^2}} \left(\lambda_{i,g}^k \frac{R_{i,g}^k}{\xi} + L_{i,g}^k \right) \right\}. \tag{26}$$

 doi:10.20944/preprints202506.2543.v1

Therefore, Problem 1 can be reformulated as

$$\begin{aligned} &\text{Problem 2:} \max_{p_{i,g}^k} \frac{1}{K} \sum_{k=1}^{K} \sum_{i=1}^{I} \sum_{g=1}^{G} \mathbf{O}_{i,g}^k \\ &\text{s.t.} (23b), (23c). \end{aligned} \tag{27}$$

Moreover, since the subproblem of outage probability involves a product of terms, it is challenging to solve directly. To address this, we apply a natural logarithm function to transform the product into a summation, thereby simplifying the problem and facilitating subsequent analysis.

$$\begin{aligned} \mathbf{E}_{i,g}^k = \ln \mathbf{O}_{i,g}^k = \mathrm{Tr} \Bigg\{ &\ln \left(\frac{\lambda_{i,g}^k R_{i,g}^k}{\xi} + L \right) \\ &+ \sum_{z=1}^{i} \frac{\sum_{j=z+1}^{I} p_{j,g}^k |h_{j,g}^k)|^2 + \sigma^2}{-p_{z,g}^k} F_{z,g}^k \Bigg\}, \end{aligned} \tag{28}$$

where $F_{z,g}^k = \frac{(2^{\frac{\hat{R}_z^g}{B}} - 1)\left((1+d_{z,g}^k)^\beta\right)}{2\mu^2}$.

Problem 2 is rewritten as

$$\begin{aligned} &\text{Problem 3:} \max_{p_{i,g}^k} \frac{1}{K} \sum_{k=1}^{K} \sum_{i=1}^{I} \sum_{g=1}^{G} \mathbf{E}_{i,g}^k \\ &\text{s.t.} (23b), (23c). \end{aligned} \tag{29}$$

Since Problem 3 is a non-convex optimization problem with respect to $p_{i,g}^k$, it is challenging to solve directly. Therefore, we adopt the SCA method, whose convergence has been proven in [11]. Hence, a lower bound for $R_{i,g}^k$ can be expressed as

$$\begin{aligned} R_{i,g}^k &= B \log_2(1 + \mathrm{SINR}_{i,g}^k) \\ &\geq B \left(a_{i,g}^k \log_2(\mathrm{SINR}_{i,g}^k) + b_{i,g}^k \right) = \hat{R}_{i,g}^k, \end{aligned} \tag{30}$$

where the equality holds when

$$a_{i,g}^k = \frac{\mathrm{SINR}_{i,g}^k}{1 + \mathrm{SINR}_{i,g}^k}, \tag{31}$$

and

$$b_{i,g}^k = \log_2(1 + \mathrm{SINR}_{i,g}^k) - a_{i,g}^k \log_2(\mathrm{SINR}_{i,g}^k). \tag{32}$$

With the fixed approximation coefficients $\mathcal{A}(k) \triangleq a_i^g(k)$ and $\mathcal{B}(k) \triangleq b_{i,g}^k$, the constraint in Problem 3 remains non-concave with respect to $p_{i,g}^k$. Therefore, we introduce the transformation $\bar{p}_{i,g}^k = \ln p_{i,g}^k$.

Here, we decompose the objective function in Problem 3 into two parts, $\mathbf{U}_{i,g}^k$ and $\mathbf{D}_{i,g}^k$, which are expressed as follows

$$\mathbf{E}_{i,g}^k = \mathrm{Tr} \left\{ \mathbf{U}_{i,g}^k + \mathbf{D}_{i,g}^k \right\}, \tag{33}$$

$$\mathbf{U}_{i,g}^k = \sum_{z=1}^{i} \frac{\sum_{j=z+1}^{I} e^{\bar{p}_{j,g}^k} |h_{j,g}^k|^2 + \sigma^2}{-e^{\bar{p}_{z,g}^k}} F_{z,g}^k, \tag{34}$$

 doi:10.20944/preprints202506.2543.v1

and

$$\begin{aligned}\mathbf{D}_{i,g}^{k} &= \ln\left(\frac{\lambda_{i,g}^{k}R_{i,g}^{k}}{\xi}+L_{i,g}^{k}\right)\\ &= \ln\left\{\frac{\lambda_{i,g}^{k}a_{i,g}^{k}\bar{p}_{i,g}^{k}|h_{i,g}^{k}|^{2}}{\xi\ln 2}+S_{i,g}^{k}\right\},\end{aligned} \tag{35}$$

where $\frac{\lambda_{i,g}^{k}a_{i,g}^{k}\ln\left(\sum_{j=i+1}^{I}e^{\bar{p}_{j,g}^{k}}|h_{j,g}^{k}|^{2}+\sigma^{2}\right)+b_{i,g}^{k}}{-\xi\ln 2}+L_{i,g}^{k}$ is abbreviated as $S_{i,g}^{k}$.

The first-order partial derivative of $\mathbf{U}_{i,g}^{k}$ is given as follows

$$\frac{\partial\mathbf{U}_{i,g}^{k}}{\partial(\bar{p}_{i,g}^{k})}=\begin{cases}\frac{|h_{i,g}^{k}|^{2}}{V_{i,g}^{k}}F_{i,g}^{k},\\ -\sum_{z=1}^{i-1}\delta_{z,g}^{k}F_{z,g}^{k}+\frac{|h_{i,g}^{k}|^{2}}{V_{i,g}^{k}}F_{i,g}^{k},\\ -\sum_{z=1}^{i-1}\delta_{z,g}^{k}F_{z,g}^{k}+\frac{\sigma^{2}}{e^{\bar{p}_{i,g}^{k}}}F_{i,g}^{k},\end{cases} \tag{36}$$

where we define $V_{i,g}^{k}=\frac{e^{\bar{p}_{i,g}^{k}}|h_{i,g}^{k}|^{2}}{\sum_{j=i+1}^{I}e^{\bar{p}_{j,g}^{k}}|h_{j,g}^{k}|^{2}+\sigma^{2}}$ and $\delta_{z,g}^{k}=\frac{e^{\bar{p}_{i,g}^{k}}|h_{i,g}^{k}|^{2}}{e^{\bar{p}_{z,g}^{k}}}$. The three cases, listed from top to bottom, correspond to $i=1$, $1<i<I$, and $i=I$, respectively.

The second-order partial derivative of $\mathbf{U}_{i}^{g}(k)$ is given by

$$\frac{\partial^{2}\mathbf{U}_{i,g}^{k}}{\partial(\bar{p}_{i,g}^{k})^{2}}=\begin{cases}-\frac{|h_{i,g}^{k}|^{2}}{V_{i,g}^{k}}F_{i,g}^{k},\\ -\sum_{z=1}^{i-1}\delta_{z,g}^{k}F_{z,g}^{k}-\frac{|h_{i,g}^{k}|^{2}}{V_{i,g}^{k}}F_{i,g}^{k},\\ -\sum_{z=1}^{i-1}\delta_{z,g}^{k}F_{z,g}^{k}-\frac{\sigma^{2}}{e^{\bar{p}_{i,g}^{k}}}F_{i,g}^{k},\end{cases} \tag{37}$$

where the three constraint conditions for the second-order partial derivatives are the same as those for the first-order.

The first and second-order derivatives of $\mathbf{D}_{i}^{g}(k)$ are expressed as follows

$$\frac{\partial\mathbf{D}_{i,g}^{k}}{\partial\bar{p}_{i,g}^{k}}=\frac{\frac{\lambda_{i,g}^{k}a_{i,g}^{k}|h_{i,g}^{k}|^{2}}{\xi\ln 2}}{\frac{\lambda_{i,g}^{k}a_{i,g}^{k}|h_{i,g}^{k}|^{2}}{\xi\ln 2}\bar{p}_{i,g}^{k}+S_{i,g}^{k}}, \tag{38}$$

$$\frac{\partial^{2}\mathbf{D}_{i,g}^{k}}{\partial\left(\bar{p}_{i,g}^{k}\right)^{2}}=\frac{-\left(\frac{\lambda_{i,g}^{k}a_{i,g}^{k}|h_{i,g}^{k}|^{2}}{\xi\ln 2}\right)^{2}}{\left(\frac{\lambda_{i,g}^{k}a_{i,g}^{k}|h_{i,g}^{k}|^{2}}{\xi\ln 2}\bar{p}_{i,g}^{k}+S_{i,g}^{k}\right)^{2}}. \tag{39}$$

 doi:10.20944/preprints202506.2543.v1

According to Equation (36), (37), (38) and (39), Problem 3 has been proven to be a convex optimization problem, and we use the dual decomposition method to solve it [29]. Consequently, the Lagrangian function for Problem 4 is

$$\begin{aligned}&\sum_{i=1}^{I}\sum_{g=1}^{G}\mathcal{L}\left(p_{i,g}^{k},\eta_{i,g}^{k},\phi_{i,g}^{k}\right)\\&=\sum_{i=1}^{I}\sum_{g=1}^{G}\mathbf{E}_{i,g}^{k}+\sum_{i=1}^{I}\sum_{g=1}^{G}\eta_{i,g}^{k}\left(p_{\max}-p_{i,g}^{k}\right)\\&+\sum_{i=1}^{I}\sum_{g=1}^{G}\phi_{i,g}^{k}\left(T_{i,g}^{max}-T_{i,g}^{total,k}\right),\end{aligned}\tag{40}$$

where $\eta_{i,g}^{k}$ and $\phi_{i,g}^{k}$ are the Lagrangian multipliers.

According to (40), the dual function $\mathcal{D}\left(\eta_{i,g}^{k},\phi_{i,g}^{k}\right)$ can be expressed as

$$\mathcal{D}\left(\eta_{i,g}^{k},\phi_{i,g}^{k}\right)=\begin{cases}\max\limits_{\bar{p}_{i,g}^{k}}\mathcal{L}\left(\bar{p}_{i,g}^{k},\eta_{i,g}^{k},\phi_{i,g}^{k}\right)\\\quad\text{s.t. }\bar{p}_{i,g}^{k}\geq 0.\end{cases}$$

Hence, the dual problem is

$$\begin{aligned}\text{Problem 4: }&\min\mathcal{D}\left(\eta_{i,g}^{k},\phi_{i,g}^{k}\right)\\&\text{s.t.}\eta_{i,g}^{k}\geq 0,\phi_{i,g}^{k}\geq 0.\end{aligned}\tag{41}$$

The power allocation $\bar{p}_{i,g}^{k}$ for the fixed values $\eta_{i,g}^{k}$, $\phi_{i,g}^{k}$ is calculated via (42) by applying KKT condition on (40). Hence, we have (see Alogorithm 4)

$$\frac{\partial\mathcal{L}\left(p_{i,g}^{k},\eta_{i,g}^{k},\phi_{i,g}^{k}\right)}{\partial\bar{p}_{i,g}^{k}}=0.\tag{42}$$

Since the problem involves solving a multi-objective nonlinear equation system where the result is equal to zero, we utilized the lsqnonlin function in MATLAB to find the optimal solution $\bar{p}_{i,g}^{*,k}$.

For $\eta_{i,g}^{k}$ and $\phi_{i,g}^{k}$, we use the gradient descent method to obtain the optimal values.

$$\eta_{i,g}^{j+1,k}=\left[\eta_{i,g}^{j,k}-\Delta\varepsilon_{1}^{j,k}(p_{\max}-p_{i,g}^{k})\right]^{+},\tag{43}$$

$$\phi_{i,g}^{j+1,k}=\left[\phi_{i,g}^{j,k}-\Delta\varepsilon_{2}^{j,k}(T_{i,g}^{max,k}-T_{i,g}^{total,k})\right]^{+}.\tag{44}$$

where j is an iteration index. The parameters $\Delta\varepsilon_1$ and $\Delta\varepsilon_2$ represent the learning rates for $\eta_{i,g}^{j}$ and $\phi_{i,g}^{j}$, respectively.

 doi:10.20944/preprints202506.2543.v1

Algorithm 4 Power Allocation Based on SCA and Dual Decomposition Methods

Input: $\lambda_{i,g}^{\text{iter},k}, \xi, \psi, \text{iter\_max}, \epsilon, D_i^g, R_{i,g}^k, \sigma, i \in \mathcal{I}, g \in \mathcal{G}$.

Initialization: $a_{i,g}^k = b_{i,g}^k = 1$, $\Delta\varepsilon = \Delta\varepsilon_2 = 0.1$, $p_{i,g}^k = p_{\max}$, $j = \text{iter} = 1$, $\mathbf{E}_i^g = \mathbf{E}_{i,g}^k = 0$.

for $k = 1$ to K **do**
  while $\Delta > \epsilon$ **or** iter $\leq$ iter_max **do**
    Update iter $=$ iter $+ 1$
    Update $a_{i,g}^k$ according formula (31)
    Update $b_{i,g}^k$ according formula (32)
    Calculate $p_{i,g}^{*,k} = \exp(\bar{p}_{i,g}^{*,k})$
    repeat
      $j = j + 1$
      Calculate $\bar{p}_{i,g}^k$ according to formula (42)
      Update $\left\{\eta_{i,g}^k\right\}$ according to formula (43)
      Update $\left\{\phi_{i,g}^k\right\}$ according to formula (44)
    until $j \geq$ iter_max
    Update $\Delta = |F(\lambda_{i,g}^{\text{iter},k}) - F(\lambda_{i,g}^{\text{iter-1},k})|$
  end while
  Obtain $\mathbf{E}_{i,g}^k$ according to formula (28)
  Update $\mathbf{E}_i^g = \mathbf{E}_i^g + \mathbf{E}_{i,g}^k$
end for

Output: $\mathbf{E}_i^g = \mathbf{E}_{i,g}^k / K$.

3.3. Complexity Analysis

The computational complexity of the proposed algorithms is analyzed as follows: For Algorithm 1, the complexity is determined by the number of iterations of the while loop, combined with the nested for loops, resulting in a time complexity of $O(t_{\max} \cdot K \cdot I \cdot G)$, where $t_{\max}$ and K represent the maximum number of iterations and the iteration count within the loop, respectively, G is the number of groups, and I is the number of sensors within each group. For Algorithm 2, the complexity is approximately $O(T \cdot N^2 \cdot G)$, where T denotes the number of iterations required to achieve a Nash-stable partition, and N represents the total number of sensors. For Algorithms 3 and 4, the complexity is $O(K \cdot L \cdot M)$, where L is the number of iterations required for convergence, and M is the number of power allocation variables. Thus, the total complexity of the system, combining the complexities of sensor grouping and power allocation processes is $O(t_{\max} \cdot K \cdot I \cdot G + T \cdot N^2 \cdot G + K \cdot L \cdot M)$.

4. Performance Evalution

In this section, we evaluate the performance of the resource allocation algorithm for minimizing outage risk under the joint optimization of remote state estimation and transmission delay. The experiments were conducted using MATLAB 2024b. The simulation setup positions the base station at coordinates $(0\,\text{m}, 0\,\text{m})$, with sensors randomly distributed within a $100\,\text{m} \times 100\,\text{m}$ area. We simulate 1000 Rayleigh fading channel realizations and use the sampled values to calculate channel gains. Each sensor is assigned a bandwidth of 1 KHz for data transmission. Specific parameters are provided in Table 1.

 doi:10.20944/preprints202506.2543.v1

Table 1. Summary of the simluation parameters

Parameters	Values
Simulation area size	100m * 100m
Base station antenna location	(0, 0)m
CPU cycles required to process task I_i^g	1000 Megacycles
Computational capability of sensor F^s	1 GHz
Computational capability of base station F^b	10 GHz
System bandwith B	1 KHz
Minimum transmission Rate $\hat{R}$	100 bps
Maximun power $p_{\max}$	20 dBm
Maximum tolerable transmission delay $T_{i,g}^{max}$	0.1 s
Size of Received Input Data D_i^g	80 B
Noise power density σ	-170 dBm/Hz
$A_i^g, C_i^g, Q_i^g, R_i^g$	[0.5, -1.5]
ξ, ψ, μ	0.4, 1, 1

For the sensor grouping algorithm, we evaluate two alternative strategies and compare them with the proposed heuristic algorithm, which optimizes sensor grouping under fixed power constraints to minimize the state estimation outage risk. The two strategies are random sensor grouping [30] and a suboptimal grouping approach [31]. The suboptimal strategy operates as follows: given N sensors, they are first sorted in descending order based on their channel gains. The sorted sensors are then evenly divided into M blocks. Sensors from the same position in each block form a group (e.g., the first sensor in each block forms the first group, the second sensor forms the second group, etc.) until all groups are created. For the power allocation algorithm, we compare two approaches: random power allocation within the allowable range [32] and assigning the maximum power value to all sensors [33]. Comparing the algorithm with the four aforementioned algorithms helps evaluate the performance, computational complexity, and practical feasibility of different strategies in the uplink NOMA system, thereby optimizing resource allocation.

Figure 2 presents the sum of the expected function in Problem 4 with 9 sensors and 3 channels. The simulation parameters are set as $\xi = 0.5$, $\hat{R} = 100$bps, $B = 1$KHZ and $p_{\max} = 20$dBm. We compare different sensor grouping strategies, including the proposed coalition game-based intelligent grouping algorithm, the random grouping algorithm, and the suboptimal grouping algorithm. As shown, across all time slots k, the coalition game-based algorithm consistently outperforms the other two in solving the sum of expectations in Problem 1. Each point is obtained from 500 Monte Carlo simulations per algorithm per time slot.

 doi:10.20944/preprints202506.2543.v1

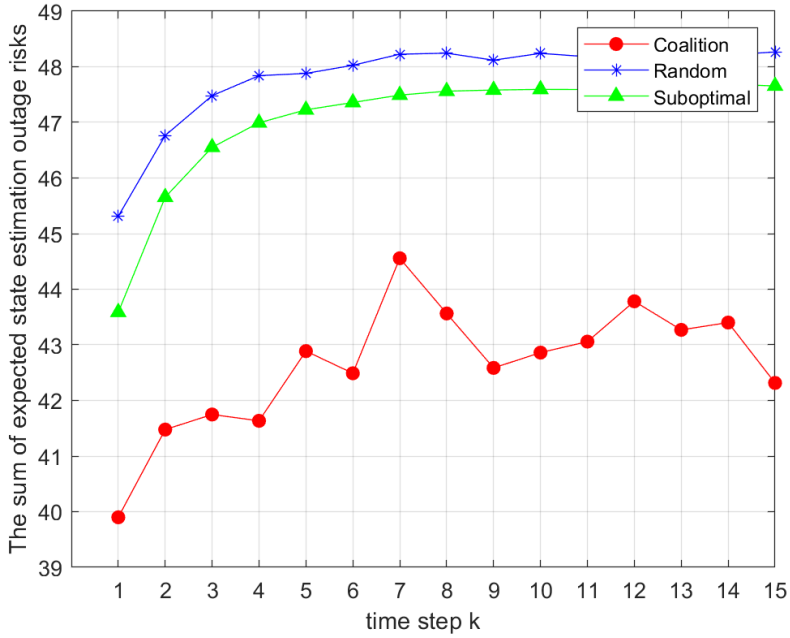

Figure 2. Comparison of the total outage risks under different sensor grouping strategies

Figure 3 compares different power allocation methods under the same coalition game-based grouping strategy. Simulation settings and Monte Carlo parameters are consistent with those in Figure 2. The joint Dinkelbach algorithm, the SCA algorithm, and the KKT-based power allocation are evaluated against random and full power allocation. The proposed joint allocation methods clearly outperform the baselines in solving the sum of expectations in Problem 1.

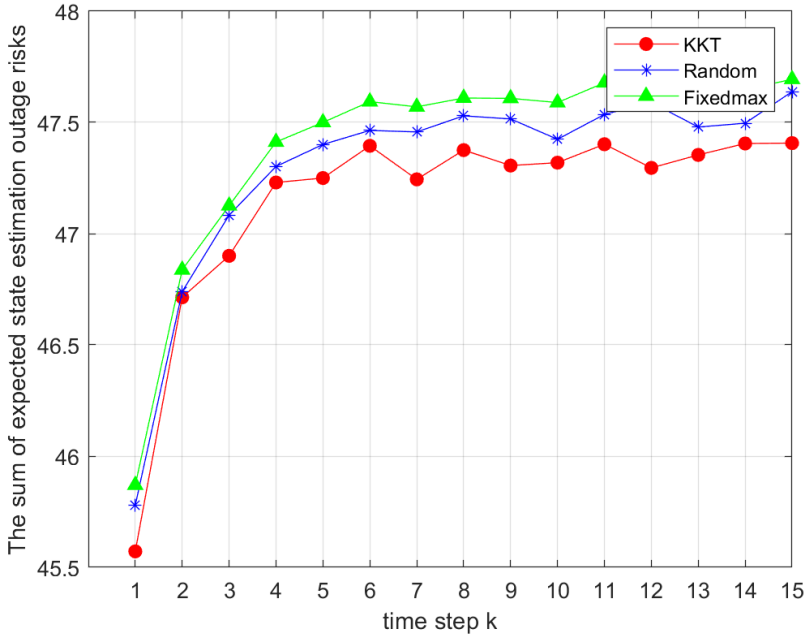

Figure 3. Comparison of the total outage risks under different power allocation strategies

Figure 4 illustrates the impact of different minimum transmission rates on the total value of the objective function in Problem 1. The minimum rate is set to 100bps, 500bps, 1000bps, while other parameters remain unchanged. It is observed that the total objective value increases significantly with $\hat{R}_{i,g'}^{k}$ which aligns with the theoretical expectations based on Equation (25).

 doi:10.20944/preprints202506.2543.v1

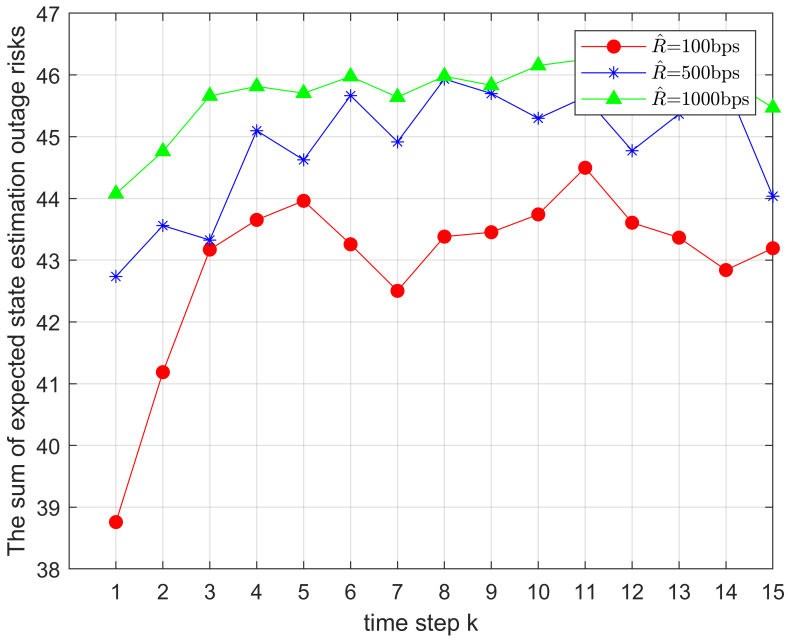

Figure 4. Comparison of the total outage risks under different minimum transmission rates $\hat{R}$.

Figure 5 examines the effect of bandwidth B on $\mathbf{J}_{i,g}^k$. Bandwidth values are set to 1KHz, 10KHz, 100KHz. The curves show that as B increases, $\mathbf{J}_{i,g}^k$ grows accordingly. Limited bandwidth constrains communication performance, while a larger B improves transmission rates and system efficiency, validating the model's sensitivity to bandwidth variations.

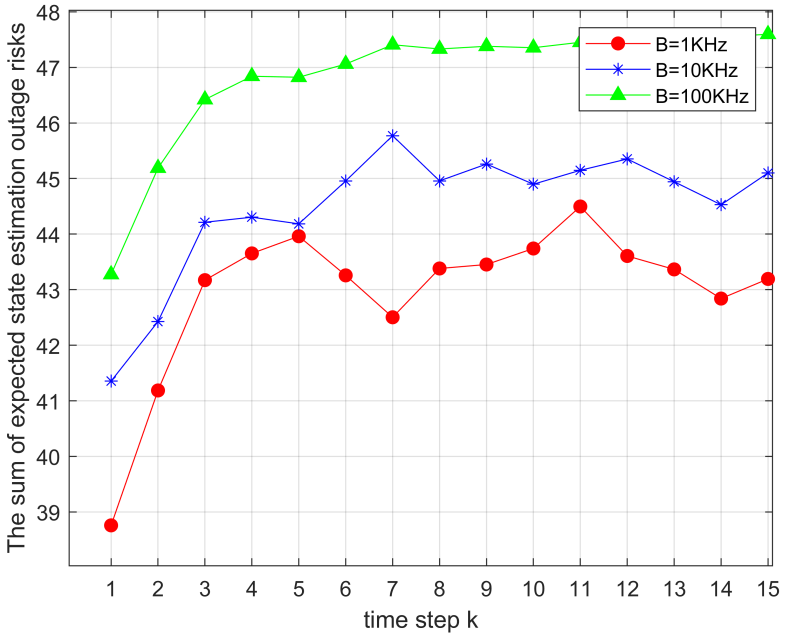

Figure 5. Comparison of the total outage risks under different bandwidths B.

In Figure 6, we investigate the impact of the weighting parameter ξ on the total value $\mathbf{J}_{i,g}^k$ of the objective function in Problem 1. Specifically, we vary the parameter ξ with values $\xi = 0.2$, $\xi = 0.5$, and $\xi = 0.8$. The results indicate a clear trend: as the proportion allocated to ξ increases, the total value $\mathbf{J}_{i,g}^k$ also rises. This suggests that in the joint optimization of remote state estimation using KF and the offloading time consumption, the latter has a more pronounced influence on the objective

 doi:10.20944/preprints202506.2543.v1

function. Given that our optimization problem aims to minimize the objective function, this result highlights a critical trade-off. To achieve optimal system performance, it is advisable to assign a relatively smaller weight to offloading time consumption while allocating a greater proportion to the remote state estimation component. This allocation strategy aligns with the objective of minimizing the overall efficiency and benefit of the system.

In Figure 6, the impact of the weighting parameter ξ on $\mathbf{J}_{i,g}^{k}$ is investigated. We consider 0.2, 0.5, 0.8. The results show that as ξ increases, the total objective value rises. This indicates that offloading time consumption has a greater influence on the objective, suggesting that assigning a smaller weight to offloading time can better optimize system performance.

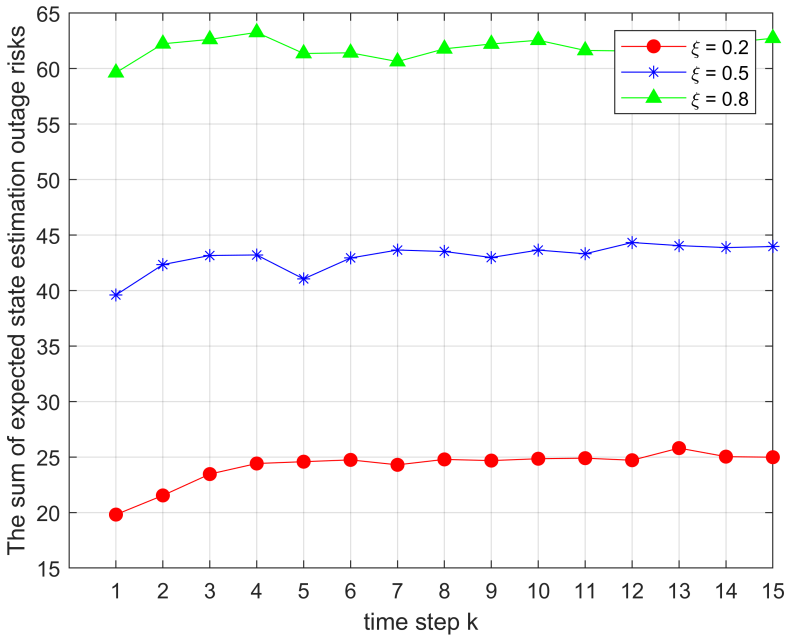

Figure 6. Comparison of total outage risks under different association factors ξ

Figure 7 analyzes the impact of maximum transmission power on $\mathbf{J}_{i,g}^{k}$. As $p_{\max}$ increases, the total objective value decreases. This is because higher transmission power strengthens the transmitted signal, thereby improving transmission reliability according to the Shannon-Hartley theorem. However, the resulting increase in power consumption must be considered in practical applications to balance performance and energy efficiency.

 doi:10.20944/preprints202506.2543.v1

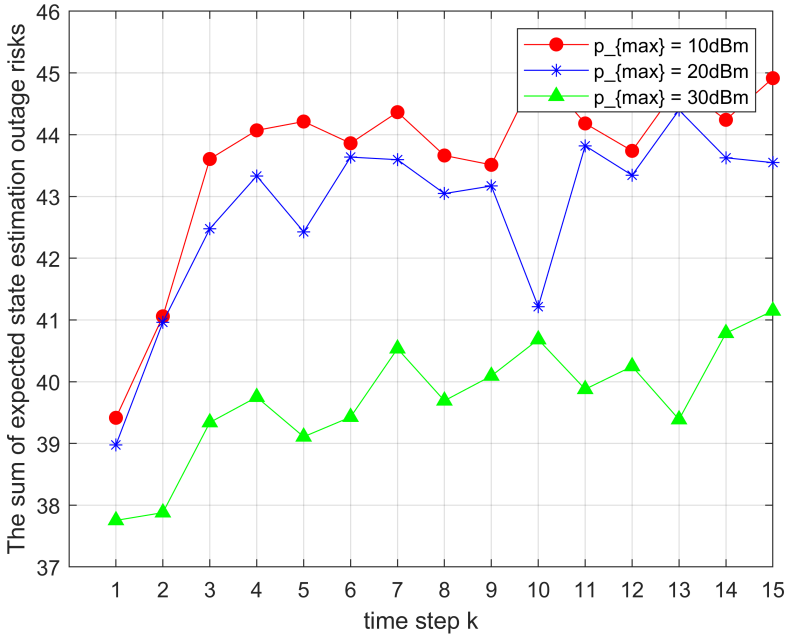

Figure 7. Comparison of total outage risks under different maximum powers $p_{\max}$

In Figure 8, we analyze how different sensor allocations within each channel group affect $\mathbf{J}_{i,g}^{k}$ with a fixed total of 12 sensors. Group sizes of 2, 3, and 4 sensors are compared. The results show that increasing the number of sensors per group improves system performance by reducing the total objective value. However, it significantly increases computational complexity, with computation time for 4 sensors per group being approximately 10 times higher than for 2 or 3 sensors. Thus, a trade-off between performance and computational cost must be carefully considered.

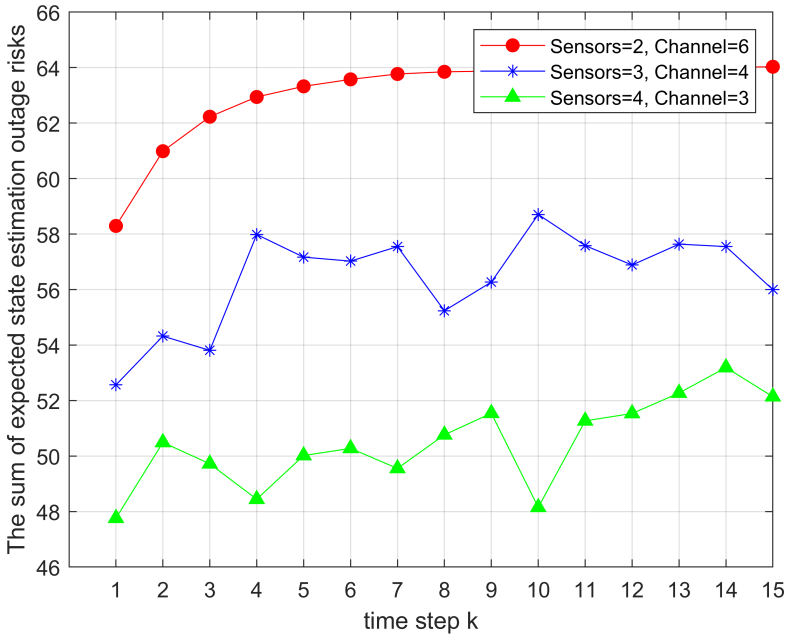

Figure 8. Comparison of total outage risks under different sensor counts within the same channel

5. Conclusions

This paper investigates the problem of minimizing outage risk under joint optimization of remote state estimation and transmission delay. By formulating the problem as a MINLP problem, it is further

 doi:10.20944/preprints202506.2543.v1

divided into an intelligent sensor grouping algorithm based on coalition game theory and a joint power allocation algorithm leveraging the Dinkelbach algorithm, SCA, and dual decomposition methods. Simulation results demonstrate that the proposed algorithm outperforms traditional sensor grouping and power allocation algorithms in terms of performance, effectively reducing the outage risk of sensors during transmission. Future research can further extend to multi-sensor and multi-base station scenarios in downlink NOMA systems, exploring outage risk assessment methods in more complex systems.

References

1. Salama, R.; Al-Turjman, F.; Bordoloi, D.; Yadav, S.P. Wireless Sensor Networks and Green Networking for 6G communication- An Overview. In Proceedings of the 2023 International Conference on Computational Intelligence, Communication Technology and Networking (CICTN), 2023, pp. 830–834. https://doi.org/10.1109/CICTN57981.2023.10141262.
2. Khan, W.U.; Jameel, F.; Jamshed, M.A.; Pervaiz, H.; Khan, S.; Liu, J. Efficient power allocation for NOMA-enabled IoT networks in 6G era. *Physical Communication* **2020**, *39*, 101043. https://doi.org/https://doi.org/10.1016/j.phycom.2020.101043.
3. Sarma, S.S.; Sachan, A.; Hazra, R.; Talukdar, F.A.; Mukherjee, A.; Chatterjee, P.; Al-Numay, W. D2D Communication in a 5G mm-Wave Cellular Network for Wireless Sensor Networks. *IEEE Sensors Journal* **2024**, *24*, 5512–5521. https://doi.org/10.1109/JSEN.2023.3300586.
4. Rathod, T.; Gupta, R.; Nehra, A.; Kumar Jadav, N.; Nehra, A. AI and Coalition Game Interplay for Efficient Resource Allocation in D2D Communication. In Proceedings of the GLOBECOM 2023 - 2023 IEEE Global Communications Conference, 2023, pp. 3058–3063. https://doi.org/10.1109/GLOBECOM54140.2023.10437084.
5. Hu, H.; Ma, C.; Tang, B. Channel Allocation Scheme for Ultra-Dense Femtocell Networks: Based on Coalition Formation Game and Matching Game. In Proceedings of the 2019 IEEE MTT-S International Wireless Symposium (IWS), 2019, pp. 1–3. https://doi.org/10.1109/IEEE-IWS.2019.8803970.
6. Chen, W.; Zhao, S.; Zhang, R.; Yang, L. Generalized User Grouping in NOMA Based on Overlapping Coalition Formation Game. *IEEE Journal on Selected Areas in Communications* **2021**, *39*, 969–981. https://doi.org/10.1109/JSAC.2020.3018832.
7. Liu, G.; Wang, R.; Zhang, H.; Kang, W.; Tsiftsis, T.A.; Leung, V.C.M. Super-Modular Game-Based User Scheduling and Power Allocation for Energy-Efficient NOMA Network. *IEEE Transactions on Wireless Communications* **2018**, *17*, 3877–3888. https://doi.org/10.1109/TWC.2018.2817194.
8. Liu, B.; Su, Z.; Xu, Q. Game theoretical secure wireless communication for UAV-assisted vehicular Internet of Things. *China Communications* **2021**, *18*, 147–157. https://doi.org/10.23919/JCC.2021.07.012.
9. Wang, D.; Huang, J.; He, M.; Huang, C. Spectrum Transaction Games for UAV Assisted Communications. *IEEE Wireless Communications Letters* **2022**, *11*, 1–1. https://doi.org/10.1109/LWC.2022.3161387.
10. Yang, Q.; Zhang, Q.; Peng, Y. Cluster-Based Strategy for Maximizing the Sum-Rate of a Distributed Reconfigurable Intelligent Surface (RIS)-Assisted Coordinated Multi-Point Non-Orthogonal Multiple-Access (CoMP-NOMA) System. *Sensors* **2024**, *24*. https://doi.org/10.3390/s24113644.
11. Xu, L.; Zhou, Y.; Wang, P.; Liu, W. Max-Min Resource Allocation for Video Transmission in NOMA-Based Cognitive Wireless Networks. *IEEE Transactions on Communications* **2018**, *66*, 5804–5813. https://doi.org/10.1109/TCOMM.2018.2854584.
12. Azarhava, H.; Musevi Niya, J. Energy Efficient Resource Allocation in Wireless Energy Harvesting Sensor Networks. *IEEE Wireless Communications Letters* **2020**, *9*, 1000–1003. https://doi.org/10.1109/LWC.2020.2978049.
13. Liu, M.; Wu, Q.; Wang, Z.; Zhao, B.; Zhang, L.; Li, J.; Zhu, X. Optimal power allocation strategy for scaled hydrogen storage system considering power-efficiency coupling relationship. In Proceedings of the 2023 IEEE Sustainable Power and Energy Conference (iSPEC), 2023, pp. 1–5. https://doi.org/10.1109/iSPEC58282.2023.10403033.
14. Zamani, M.R.; Eslami, M.; Khorramizadeh, M.; Zamani, H.; Ding, Z. Optimizing Weighted-Sum Energy Efficiency in Downlink and Uplink NOMA Systems. *IEEE Transactions on Vehicular Technology* **2020**, *69*, 11112–11127. https://doi.org/10.1109/TVT.2020.3007716.

 doi:10.20944/preprints202506.2543.v1

15. Zuo, H.; Tao, X. Power allocation optimization for uplink non-orthogonal multiple access systems. In Proceedings of the 2017 9th International Conference on Wireless Communications and Signal Processing (WCSP), 2017, pp. 1–5. https://doi.org/10.1109/WCSP.2017.8171176.
16. Zhang, Q.; An, K.; Yan, X.; Xi, H.; Wang, Y. User Pairing for Delay-Limited NOMA-Based Satellite Networks with Deep Reinforcement Learning. *Sensors* **2023**, *23*. https://doi.org/10.3390/s23167062.
17. Feng, J.; Yu, F.R.; Pei, Q.; Du, J.; Zhu, L. Joint Optimization of Radio and Computational Resources Allocation in Blockchain-Enabled Mobile Edge Computing Systems. *IEEE Transactions on Wireless Communications* **2020**, *19*, 4321–4334. https://doi.org/10.1109/TWC.2020.2982627.
18. Dixit, S.; Shukla, V.; Misra, M.K.; Jimenez, J.M.; Lloret, J. Progressive Pattern Interleaver with Multi-Carrier Modulation Schemes and Iterative Multi-User Detection in IoT 6G Environments with Multipath Channels. *Sensors* **2024**, *24*. https://doi.org/10.3390/s24113648.
19. Tabee Miandoab, F.; Fazel, M.S.; Mahdavi, M. Outage Analysis of Multiuser MIMO-NOMA Transmissions in Uplink Full-Duplex Cooperative System. *IEEE Wireless Communications Letters* **2022**, *11*, 2076–2079. https://doi.org/10.1109/LWC.2022.3193489.
20. Lu, H.; Xie, X.; Shi, Z.; Cai, J. Outage Performance of CDF-Based Scheduling in Downlink and Uplink NOMA Systems. *IEEE Transactions on Vehicular Technology* **2020**, *69*, 14945–14959. https://doi.org/10.1109/TVT.2020.3031367.
21. Lu, H.; Xie, X.; Shi, Z.; Kadoch, M.; Cheriet, M.; Cai, J. Outage Probability of CDF-Based Scheduling for Uplink NOMA with Practical SIC Considerations. In Proceedings of the 2020 International Wireless Communications and Mobile Computing (IWCMC), 2020, pp. 1031–1036. https://doi.org/10.1109/IWCMC48107.2020.9148410.
22. Yadav, P.; Jain, S. Outage Probability Analysis of IRS-Assisted NOMA System Over Rician Fading Channel. 06 2024, pp. 1–6. https://doi.org/10.1109/ICCCNT61001.2024.10725143.
23. Zhang, N.; Wang, J.; Kang, G.; Liu, Y. Uplink Nonorthogonal Multiple Access in 5G Systems. *IEEE Communications Letters* **2016**, *20*, 458–461. https://doi.org/10.1109/LCOMM.2016.2521374.
24. Basha, S.T.; Nageena Parveen, S.; Bathini, A.; Gade, S.S.; Kothapelly, V. Outage Analysis of Downlink Cooperative SWIPT -NOMA system with optimum energy harvesting and imperfect CSI. In Proceedings of the 2024 15th International Conference on Computing Communication and Networking Technologies (ICCCNT), 2024, pp. 1–6. https://doi.org/10.1109/ICCCNT61001.2024.10724539.
25. Trankatwar, S.; Wali, P. Optimal Power Allocation for Downlink NOMA Heterogeneous Networks to Improve Sum Rate and Outage Probability. In Proceedings of the 2022 IEEE India Council International Subsections Conference (INDISCON), 2022, pp. 1–6. https://doi.org/10.1109/INDISCON54605.2022.9862842.
26. Li, Y.; Quevedo, D.E.; Lau, V.; Shi, L. Online sensor transmission power schedule for remote state estimation. In Proceedings of the 52nd IEEE Conference on Decision and Control, 2013, pp. 4000–4005. https://doi.org/10.1109/CDC.2013.6760501.
27. Li, Y.; Mehr, A.S.; Chen, T. Multi-sensor transmission power control for remote estimation through a SINR-based communication channel. *Automatica* **2019**, *101*, 78–86. https://doi.org/https://doi.org/10.1016/j.automatica.2018.11.039.
28. Pang, G.; Liu, W.; Li, Y.; Vucetic, B. Deep Reinforcement Learning for Radio Resource Allocation in NOMA-based Remote State Estimation. In Proceedings of the GLOBECOM 2022 - 2022 IEEE Global Communications Conference, 2022, pp. 3059–3064. https://doi.org/10.1109/GLOBECOM48099.2022.10001377.
29. Boyd, S.; Vandenberghe, L. *Convex Optimization*; Cambridge University Press, 2004.
30. Ahmad, A.W.; Mehmood Bahadar, N. Exploiting Heterogeneous Networks model for Cluster Formation and Power Allocation in Uplink NOMA. In Proceedings of the 2019 21st International Conference on Advanced Communication Technology (ICACT), 2019, pp. 129–133. https://doi.org/10.23919/ICACT.2019.8701921.
31. Mohsenivatani, M.; Liu, Y.; Derakhshani, M.; Parsaeefard, S.; Lambotharan, S. Completion-Time-Driven Scheduling for Uplink NOMA-Enabled Wireless Networks. *IEEE Communications Letters* **2020**, *24*, 1775–1779. https://doi.org/10.1109/LCOMM.2020.2987639.
32. Duan, Z.; Yang, X.; Xu, Q.; Wang, L. Covert Communication in Uplink NOMA Systems Against a Two-Phase Detector. In Proceedings of the GLOBECOM 2022 - 2022 IEEE Global Communications Conference, 2022, pp. 5516–5521. https://doi.org/10.1109/GLOBECOM48099.2022.10001211.
33. Li, Y.; Quevedo, D.E.; Lau, V.; Shi, L. Multi-sensor transmission power scheduling for remote state estimation under SINR model. In Proceedings of the 53rd IEEE Conference on Decision and Control, 2014, pp. 1055–1060. https://doi.org/10.1109/CDC.2014.7039521.

 doi:10.20944/preprints202506.2543.v1